Adsorption-Concentration Polarization Model for Ultrafiltration in Mixed Matrix Membrane

Sourav Mondal, Raka Mukherjee, Somak Chatterjee, and Sirshendu De
Dept. of Chemical Engineering, Indian Institute of Technology Kharagpur, Kharagpur, West Bengal 721302, India

DOI 10.1002/aic.14420
Published online March 1, 2014 in Wiley Online Library (wileyonlinelibrary.com)

Adsorption has been found to be significant in ultrafiltration by mixed matrix membrane. Removal of very low molecular weight solutes compared to the molecular weight cut off of the membrane is facilitated by adsorption. The modeling of the adsorption coupled with concentration polarization is presented based on the mathematical approach developed by Gekas et al. (Gekas et al. Chem Eng Sci. 1993;48:2753–2765), from the first principles. However, extensive modifications were included in theoretical development including those suggested by Ruiz-Bevia et al. (Ruiz-Bevia et al. Chem Eng Sci. 1997;52:2343–2352). The developed model captured the rejection dynamics with the help of retention factor. The model equations were solved under the framework of boundary layer analysis, using the integral approach. Effects of the adsorption isotherm and the different parameters affecting the system performance were also investigated. Further, experimental validation of the model results with two different mixed matrix ultrafiltration studies was also elucidated. © 2014 American Institute of Chemical Engineers *AIChE J*, 60: 2354–2364, 2014
Keywords: mixed matrix membrane, adsorption, concentration polarization, ultrafiltration, fluoride, catechol

Introduction

Application of mixed matrix membrane (MMM) has gained considerable interest in membrane separation for the past couple of years.[1–3] The primary reason is to have the properties of membrane tailor-made to achieve high selectivity in a particular separation process.[4,5] It has been observed that doping of inorganic filler materials onto polymeric membranes increases its selectivity retaining its high throughput. The flux decline as well as the rejection mechanism in membrane filtration is attributed to the phenomenon of concentration polarization resulting from (1) reduction in driving force due to increased osmotic pressure on the membrane surface,[6] (2) formation of gel layer which offers an additional hydraulic resistance to the overall solvent flux,[7] (3) electrokinetic effects due to the presence of charged colloids,[8] and (4) pore blocking.[9] However, contrasting to these conventional concepts, solute adsorption together with diffusion and convection in the membrane separation process plays an important role in the rejection profile as well as the permeate flux mechanism, in the MMM.

Understanding of the transport process coupled with adsorption mechanism has not been explored to a significant extent. The first reported study of adsorption on membrane was by Matthiasson, who suggested that, indeed adsorption played important role in ultrafiltration.[10] The first modeling approach was developed by Doshi (1986) combining the interplay of adsorption and concentration polarization in an unstirred batch cell.[11] He developed the model for steady state under the two limiting cases of adsorption or diffusion dominating. In case of adsorption limited process, he considered the membrane surface concentration to be negligible due to desorption of solute from the membrane to the permeate side. In case of diffusion limited process, he argued that ultrafiltration was governed by the osmotic pressure difference. Further development was carried out by Gekas et al. in 1993, in modeling of protein ultrafiltration.[12] They introduced both the adsorption and concentration polarization in the model. The model was based on the generalized concentration boundary layer equations, complemented by addition of a source term due to adsorption in the boundary condition at the membrane surface. Numerical simulation was performed for the system of equations using finite discretization. However, as pointed out by Ruiz-Bevia et al. in 1997, there were some inconsistencies in the modeling approach by Gekas et al., which were corrected and an improved version of the model was presented.[13] They argued that the evaluation for adsorption dynamics could not be solved explicitly and required coupled solution with the boundary layer equation, unlike the analysis of Gekas et al.[12] They also pointed out an inconsistency with reference to the convention in calculating the diffusive term with respect to the co-ordinate system chosen. However, their model did not include the variation of the concentration of batch volume with time. Also, quantification of the permeate concentration was not included.

In this study, a comprehensive mathematical analysis has been presented taking into the corrections suggested by Ruiz-Bevia et al.[13] for MMM. The modeling approach takes into account of the growth of the concentration boundary layer, profile of membrane surface concentration with time, development of the adsorption resistance, permeate

Correspondence concerning this article should be addressed to S. De at sde@che.iitkgp.ernet.in.
Correction added on April 4, 2014 after online publication: revised Acknowledgment section.

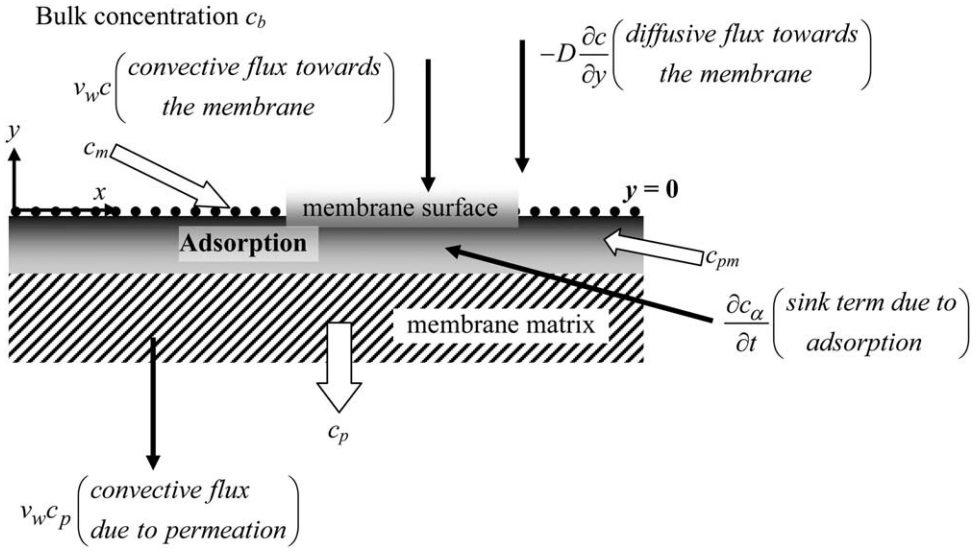

Figure 1. Schematic of the adsorption phenomena.

concentration and the variation of the feed volume, and concentration with duration of filtration. Complete state of the art analytical solution has been attempted using the integral method of solution. The set of coupled differential algebraic equations (DAE) has been solved to get the results. Finally, the model predictions have been compared with two sets of experimental results for fluoride removal using alumina-doped MMM and for catechol removal using alumina nanoparticle-doped MMM. Sensitivity analyses are also carried out for the model parameters and for the constants of adsorption isotherm.

Theoretical Development

The phenomena of concentration polarization in presence of adsorption occurring over the membrane surface have been described in Figure 1. The model equations representing the transport of solute in MMM are subjected to the following assumptions:

1. Thickness of concentration boundary layer is small, so that the transverse velocity is equal to the permeation velocity. The validity of this assumption is more consolidated in the subsequent result and discussion sections.
2. Diffusivity of the solute is constant and does not depend on concentration.
3. Because concentration boundary layer is thin, the amount of solute present within the boundary layer is small enough to be ignored.
4. The density of the feed and permeate stream are considered equal, as these solution are diluted enough to affect density.
5. The membrane density and porosity are uniform and isotropic.
6. The variation of adsorption resistance with solute adsorption is quantified following the relation as mentioned by Ruiz-Bevia et al.[13]
7. The real retention (R_r) of the membrane is constant.

In a batch experimental setup, the governing species transport equation in transient form is expressed as[12,13]

$$\frac{\partial c}{\partial t}+v\frac{\partial c}{\partial y}=D\frac{\partial^2 c}{\partial y^2} \tag{1}$$

where c is the solute concentration and y is the distance in the boundary layer above the membrane surface. As stated in the assumptions, the y-component velocity (v) is equal to the permeation velocity at the wall[14] and within thin concentration boundary layer, v is not a function of y. Thus, the y-component velocity becomes

$$v=-v_w \tag{2}$$

The initial condition for this process is

$$\text{at } t=0,\ \ c(y,0)=c_0 \tag{3}$$

with, c_0 being the initial concentration. The boundary condition at the edge of the boundary layer thickness (δ) is

$$\text{at, } y=\delta(t),\ \ c=c_b(t) \tag{4}$$

where c_b is the bulk concentration which increases with time of filtration. The other boundary condition at the fluid-membrane interface ($y=0$) is[13]

$$\text{at } y=0,\ \ v_w(c_m-c_p)=D\left.\frac{\partial c}{\partial y}\right|_{y=0}+\left.\frac{dc_\alpha}{dt}\right|_{y=0} \tag{5}$$

where c_α represent the amount of solute adsorbed by the membrane surface, c_m is the membrane surface concentration ($c_m=c|_{y=0}$), and c_p is the downstream permeate concentration. It may be noted here, that in mass-transfer analysis, the diffusive flux $D\frac{\partial c}{\partial y}|_{y=0}$, which accounts for the concentration polarization is always away from the membrane (in the form of back diffusion) as the solute concentration over the membrane surface is higher than the bulk concentration. However, this may not be true in case of strong adsorption occurring in the membrane surface as in the case of MMM. As adsorption is equilibrium governed process, the solutes polarized over membrane surface gets adsorbed by the membrane and in the process, the surface concentration decreases. Hence, more solutes get diffused from the bulk toward the membrane surface, due to positive concentration gradient.[15]

Another interesting aspect observed during ultrafiltration of proteins (or other high-molecular weight components) is that both concentration polarization and adsorption work competitively leading to deposition of solute particles over the membrane surface. In such situations, there exists a

particular transition time, when the concentration polarization due to back diffusion becomes prominent over adsorption. In such situation, Eq. 5 is transformed to Eq. 6

$$\text{at } y=0,\ \ v_w\left(c_m-c_p\right)+D\left.\frac{\partial c}{\partial y}\right|_{y=0}=0 \tag{6}$$

The permeate flux across the membrane at any point of time can be expressed as[13]

$$v_w(t)=\frac{\Delta P-\Delta\pi}{R_m+R_{ad}(t)} \tag{7}$$

where $R_{ad}(t)$ is the adsorption resistance and is described later on. The osmotic pressure (π) is calculated considering it as an ideal solution (similar to salts) using the Vant-Hoff's relation[16]

$$\pi=\left(\gamma^+ +\gamma^-\right)\frac{R_g T}{M_W}c \tag{8}$$

It is to be noted that one can introduce typical polynomial dependence of osmotic pressure with concentration for macromolecular solutes.[17] This particular linear functionality has been used to reduce the mathematical complexity and to simulate the results of ultrafiltration of a fluoride salt and another low molecular weight organic solute.

Thus, osmotic pressure difference ($\Delta\pi$) is represented as

$$\Delta\pi=\pi|_m-\pi|_p=\left(\gamma^+ +\gamma^-\right)\frac{R_g T}{M_W}\left(c_m-c_p\right) \tag{9}$$

The bulk solute concentration can be evaluated considering an overall species balance[18]

$$\frac{d}{dt}\left(c_b V\right)+A_m\left(\frac{dc_\alpha}{dt}+\int_0^\delta c(y,t)dy+c_p v_w\right)=0 \tag{10}$$

By carefully observing the order of magnitude of the terms, one can very well ignore $\int_0^\delta c(y,t)dy$, as thickness concentration boundary layer, δ is very small. Thus, Eq. 10 becomes

$$V\frac{dc_b}{dt}+c_b\frac{dV}{dt}+A_m\left(\frac{dc_\alpha}{dt}+c_p v_w\right)=0 \tag{11}$$

Considering an overall material balance, the governing equation for the retentate volume (V) can be obtained

$$\frac{dV}{dt}=-v_w A_m \tag{12}$$

It has been assumed that the density in the retentate and permeate side are equal, as it is dilute solution and density is a weak function of concentration. The initial condition for Eq. 11 and Eq. 12 is

$$\text{at } t=0,\quad c_b=c_0 \text{ and } V=V_0 \tag{13}$$

Quantification of adsorption

The dynamics of adsorption phenomena can be quantified using the following expression[12]

$$\frac{dc_\alpha}{dt}=\alpha_1 c^{\alpha_2}\left[c_e-c_\alpha\right] \tag{14}$$

where c_e is the adsorption equilibrium concentration on the membrane surface (adsorbent), represented by the Langmuir isotherm as

$$c_e(t)=\frac{Ac}{1+Bc} \tag{15}$$

In the above equation, A and B are isotherm constants and c is the solute concentration evaluated at the membrane surface (c_m). The standard Langmuir isotherm model is represented by

$$q_e=\frac{k_a\ V_m\ c}{1+k_a\ c} \tag{16}$$

Comparing the above expression with Eq. 15 one can identify that

$$A=k_a V_m \rho_{memb}(1-\varepsilon)L \tag{17a}$$

and

$$B=k_a \tag{17b}$$

Because c_e in Eq. 15 is in kg/m^2 and c_m is in kg/m^3, the constants A and B have to be in appropriate units. It can be mentioned that a different adsorption isotherm model, such as Freundlich or Tempkin can also be chosen. In this model, Langmuir isotherm is selected, as this widely represents adsorption phenomena for many equilibrium governed mass-transfer processes. Also, as far as the applicability and validity of the model is concerned, both the sets of experimental results follow Langmuir adsorption isotherm.

The adsorption resistance, R_{ad}, which depends on the adsorption concentration is represented as[13]

$$R_{ad}(t)=k' c_\alpha^n \tag{18}$$

where k' and n are model parameters specific to the particular membrane-solute system.

Definition of the real retention (R_r)

The adsorption phenomena across the membrane matrix can be visualized as a two stage sequential process. Interplay of various transport mechanisms at the membrane-feed solution interface and at the membrane-permeate side interface is described in Figure 1. Considering the retention across the membrane-feed solution interface, a real retention factor can be defined as

$$R_{r1}=1-\frac{c_{pm}}{c_m} \tag{19}$$

while the retention across the membrane-permeate interface is described as

$$R_{r2}=1-\frac{c_p}{c_{pm}} \tag{20}$$

Thus, using Eqs. 19 and 20, the concentration across the membrane surface (c_m) and permeate side (c_p) is related as

$$\frac{c_p}{c_m}=(1-R_{r1})(1-R_{r2})=1-R_r \tag{21}$$

where $R_r=(R_{r1}+R_{r2})-R_{r1}R_{r2}$. This retention factor is specific to the particular membrane-solute system, which is assumed constant in the present study.

Solution of the model equations

The species transport equation in the boundary layer, considering $v=-v_w$ as obtained from Eq. 1 is

$$\frac{\partial c}{\partial t} - v_w \frac{\partial c}{\partial y} = D \frac{\partial^2 c}{\partial y^2} \tag{22}$$

Nondimensionalizing the above equation, we get

$$\frac{\partial c^*}{\partial \tau} - Pe_w \frac{\partial c^*}{\partial y^*} = \frac{\partial^2 c^*}{\partial y^* 2} \tag{23}$$

where $Pe_w = \frac{v_w R}{D}$; $y^* = \frac{y}{R}$; $\tau = \frac{tD}{R^2}$; $\delta^* = \frac{\delta}{R}$ and $c^* = c/c_0$. Consequently, the boundary conditions expressed in Eqs. 3 and 4 are cast in nondimensional form as

$$\text{at } \tau = 0, \quad c^* = 1 \tag{24}$$

and

$$\text{at } y^* = \delta^*, \quad c^* = c_b^* \tag{25}$$

From the definition of the membrane surface concentration

$$\text{at } y^* = 0, \quad c^* = c_m^* \tag{26}$$

Now, following an integral method of solution of the one-dimensional parabolic PDE (Eq. 23),[14] the concentration profile is defined (within the mass-transfer boundary layer) as

$$c^* = a_0 + a_1 y^* + a_2 y*^2 \tag{27}$$

Using the condition presented in Eqs. 24–26, the constants a_0, a_1, and a_2 are calculated. Thus, the concentration profile is expressed as

$$c^* = c_m^* - 2(c_m^* - c_b^*)\left(\frac{y^*}{\delta^*} - \frac{y*^2}{2\delta*^2}\right) \tag{28}$$

Differentiating Eq. 28 with respect to $y*$ and τ, and substituting the derivatives in Eq. 23, the following expression is obtained

$$\begin{aligned} &\frac{1}{2(c_m^* - c_b^*)}\left(1 - 2\frac{y^*}{\delta^*} + \frac{y*^2}{\delta*^2}\right)\frac{dc_m^*}{d\tau} + \left(\frac{y^*}{\delta^*} - \frac{y*^2}{2\delta*^2}\right)\frac{dc_b^*}{d\tau} \\ &+ \left(\frac{y^*}{\delta*^2} - \frac{y*^2}{\delta*^3}\right)\frac{d\delta^*}{d\tau} - Pe_w\left(\frac{y*}{\delta*^2} - \frac{1}{\delta^*}\right) = \frac{1}{\delta*^2} \end{aligned} \tag{29}$$

Taking the zeroth moment of above equation by multiplying both sides by $dy*$ and integrating across the boundary layer thickness from zero to $\delta*$, results the following expression

$$\frac{\delta^*}{2(c_m^* - c_b^*)}\left(1 - \frac{2\delta^*}{3}\right)\frac{dc_m^*}{d\tau} + \frac{\delta^*}{3}\frac{dc_b^*}{d\tau} + \frac{\delta^*}{6}\frac{d\delta^*}{d\tau} + \frac{Pe_w \delta^*}{2} = 1 \tag{30}$$

The above differential equation couples the dynamics of development of the concentration boundary layer, evolution of the membrane surface, and bulk solute concentration. The nondimensional form of the equations representing the flux at the interface (Eq. 5), adsorption dynamics (Eq. 14), interface equilibrium concentration (Eq. 15), adsorption resistance (Eq. 18), permeate flux (Eq. 6), and the change of retentate concentration and volume with time (Eqs. 11 and 12) is presented in the appendix.

Therefore, the system of DAE constituting Eq. 30 and Eqs. A1–A7 have been solved numerically using the MATLAB, by invoking the state independent mass-matrix.[19] The initial value for $\delta*$ is obtained from the asymptotic solution of Eq. 30 in the limiting case of $\tau \to 0$, considering without any adsorption, using the procedure outlined by De et al.[14]

$$\delta^*|_{\tau \to 0} = \sqrt{12\ \tau} \tag{31}$$

This is necessary to start the solution (initial τ is a very small nonnegative number other than zero) and the system of equation becomes stable. The initial condition for Pe_w is corresponds to pure water flux. Thus, the profiles of V^*, Pe_w, c_b^*, c_m^*, $\delta*$, c_α^* have been computed for various operating conditions.

Determination of the unknown parameters

The objective function (S_1) for error minimization of permeate flux is

$$S_1 = \sum_{i=1}^{N_{exp}} \sum_{j=1}^{N_d} \left(\frac{v_{w,exp}^{j,i} - v_w^{j,i}}{v_{w,exp}^{j,i}}\right) \tag{32}$$

and for the retention is

$$S_2 = \sum_{i=1}^{N_{exp}} \sum_{j=1}^{N_d} \left(\frac{R_{0,exp}^{j,i} - R_0^{j,i}}{R_{0,exp}^{j,i}}\right) \tag{33}$$

The model constants (k, n, α_1, α_2) are evaluated by simultaneously optimizing the experimental profiles of permeate flux and rejection ($S_1 + S_2$).[20,21] The sum of the squares of the relative error between the experimental and simulated profiles is minimized using an optimization routine of interior point algorithm following a trust region method.[22] The value of R_r is obtained by optimizing the rejection profiles for all sets of experimental data corresponding to a specific membrane-solute system (S_2).

Experimental Details

Materials

MMM were prepared by phase inversion technique using cellulose acetate phthalate (CAP) as the base polymer. CAP was purchased from GM Chemicals Company Limited, Mumbai, India. *N*, *N* Dimethyl formamide (DMF) was procured from Merck, Mumbai, India. The alumina nanoparticle was provided by US Research Nanomaterials, Houston. Catechol and sodium fluoride (NaF) were obtained from Merck, Mumbai, India.

Preparation of the CAP-alumina nanoparticle doped MMM

The polymer casting solution was prepared by doping 20% w/w alumina nanoparticle in the solvent (DMF) at 60°C. Then, CAP, which was a nanoparticle stabilizer itself, in 15% by weight, was added slowly to the suspension while stirring continuously. The mixture was then sonicated for 6 h with occasional stirring to prevent agglomeration of nanoparticle. Nonwoven polyester fabric (product number: TNW006013, supplied by Hollytex, New York) was attached to the glass slides and was fixed by tape. The above casting solution was poured onto one end of the fiber. Manual drawdown was made with a speed of 20 mm/s using a doctor's blade set at a fixed gap of 150 μ. The membrane was put in water bath at 27°C for 16 h to complete the phase inversion. Details of the physical characteristics of the membrane (such as molecular weight cutoff, contact angle, SEM, mechanical strength, etc.) were already reported elsewhere[23] and the important properties necessary for the present simulation are mentioned in Table 1.

Table 1. Values of the Different Physical Properties of the System

Parameter	UF of Fluoride using Activated Alumina-Doped CAP Membrane	UF of Catechol using Alumina Nanoparticle-Doped CAP Membrane
Membrane permeability, L_p, (m/Pa s)	0.97×10^{-11}	1.87×10^{-11}
Membrane thickness, L, (mm)	0.72	0.7
Membrane porosity, ε	0.4	0.6
Membrane density, ρ_{memb}, (kg/m^3)	421.8	99.3
Molecular weight of the solute, M_w, (g/mol)	19	110
Diffusivity of the solute, D, (m^2/s)	1.4×10^{-9} (Ref. 24)	8.9×10^{-10} (Ref. 25)
Radius of the batch setup, R, (mm)	33 (same experimental setup)	
Viscosity of the solution, μ, (Pa s)	0.001 (solution is very dilute)	
Temperature, T, (K)	298 (room temperature)	
Additional Properties of the Membrane		
Molecular weight cut off (kDa)	24	122
Contact angle	52.3	59
Permeability (m/Pa s)	1.4×10^{-11}	1.87×10^{-11}
Adsorption Isotherm (Based on Langmuir Model) Constants		
A (m)	3.37	0.085
B (m^3/kg)	3.27	16.50

Preparation of the CAP-activated alumina composite MMM

The casting solution was prepared by doping 35% w/w of activated alumina and 20% w/w CAP as the base polymer in DMF. The casting solution was prepared by mixing CAP in preheated DMF at 45°C, very slowly. Continuous constant stirring was given to the CAP-DMF solution with intermediate heating at times just to ensure proper dissolution of CAP for 4 h. Next, alumina was added at a particular concentration and the mixture was sonicated for 6 h. The polymeric solution was cast in the similar fashion as described in previous section. Details of the physical characteristics of the membrane (such as molecular weight cutoff, contact angle, SEM, etc.) are presented elsewhere.[26]

The casting composition was chosen so that the prepared membrane exhibits maximum values of permeability, porosity, hydrophilicity, and surface zeta potential in the case of alumina nanoparticle-doped membrane. In the case of activated alumina composite membrane, the casting solution becomes too viscous beyond certain alumina content (35% w/w) and becomes infeasible for casting. For further information on the methodology of membrane fabrication, the suggested references are Refs. 23,26.

Unstirred batch cell filtration experiments

Membrane filtration experiments were conducted in unstirred batch cell at room temperature for 3 h using synthetic catechol and fluoride solution. The catechol solution was ultrafiltered using CAP-alumina nanoparticle doped MMM at pH 8.3, for different feed concentrations and operating transmembrane pressure (TMP). The permeate catechol concentration was measured using UV spectrophotometer (model: Lambda 35, supplied by M/S, Perkin Elmer, Connecticut), having peak absorbance at 277 nm.

The sodium fluoride solution was ultrafiltered using CAP-activated alumina composite MMM for different feed concentration and TMP. The experiments were conducted at room temperature and pH 7.0. The fluoride concentration in the permeate stream was measured using an ion specific electrode (model: Orion 720A+, Thermo Electron Corporation, Beverly). The schematic of the experimental setup is presented in Figure 2.

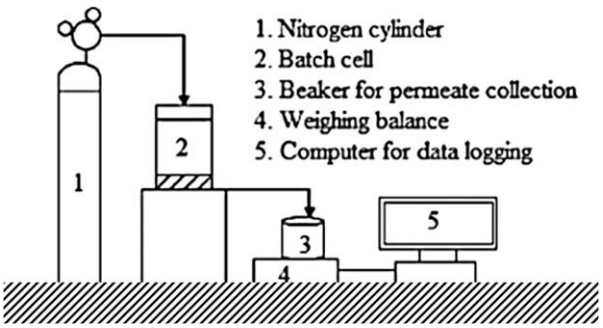

Figure 2. Schematic of the experimental setup.

Results and Discussion

The validation of the theoretical model analysis was carried out for two different membrane solute systems. The first one is ultrafiltration of fluoride contaminated water using CAP-doped alumina MMM as explained in the experimental section. The second one is ultrafiltration of catechol using alumina nanoparticles-doped CAP membrane. The values of the physical properties and adsorption isotherm constants of the system used in the simulation are described in Table 1. The typical parameters optimized for these two separate systems are presented in Table 2. The profiles of Pe_w, c_b^*, V^*, c_m^*, δ^*, c_α^*, and c_p^* are obtained by solving the system of DAE (Eq. 30 and Eqs. A1–A7) as already described. The simulation results for the profiles of the different internal variables of interest are presented in Figures 3–6, corresponding to the UF of fluoride using the optimized model parameter values.

The effect of the feed concentration of fluoride and TMP drop on the development of the concentration boundary layer

Table 2. Optimized Values of the Model Parameters

Parameter	UF of Fluoride using Alumina-Doped CAP Membrane	UF of Catechol using Nanoparticle Alumina-Doped CAP Membrane
k	$(2.50 \pm 0.12) \times 10^{14}$	$(3.90 \pm 0.20) \times 10^{13}$
n	0.12 ± 0.006	0.10 ± 0.005
α_1 (m^3/kg s)	$(1.00 \pm 0.05) \times 10^{-6}$	$(1.00 \pm 0.05) \times 10^{-3}$
α_2	0.05 ± 0.002	3.00 ± 0.15
R_r	0.85 ± 0.04	0.70 ± 0.04

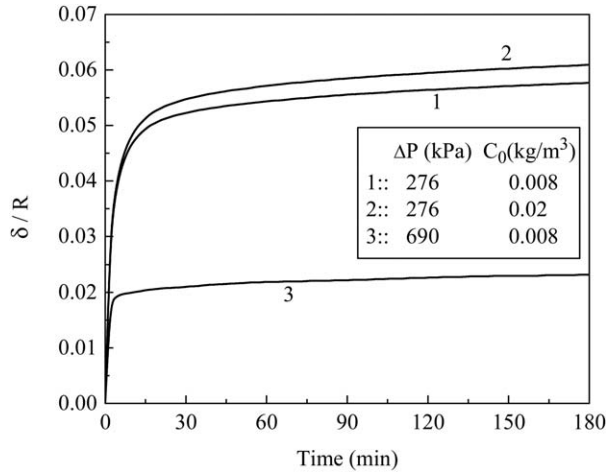

Figure 3. Variation of the concentration boundary layer thickness (δ) for different operating conditions.

thickness is shown in Figure 3. The plot shows that the thickness of the concentration boundary layer increases with feed concentration (curves 1 and 2) and decreases with TMP (curves 1 and 3). It must be noted that two interlinking phenomena occur here. One of them is concentration polarization while the other is adsorption. On increasing the TMP, one would expect higher solute polarization as explained from the classical boundary layer analysis of membrane transport phenomena.[27] Contrasting to this, in this scenario, solute adsorption by the membrane surface also plays a significant role. In fact, for MMM, solute adsorption is much more dominant compared to diffusion-controlled concentration polarization. It has to be noted that due to the effect of adsorption, the membrane surface concentration (C_m) decreases and becomes less than the bulk concentration. The effects of feed concentration are observed from the curves 1 and 2. As the feed concentration increases, solute concentration in the concentration boundary layer increases and, therefore, its thickness is also increased. Effects of TMP on thickness of concentration boundary layer are observed from curves 1 and 3. Both of these curves are at the same feed concentration. With increase in TMP, more solutes are convected toward the membrane surface, thereby, increasing the rate of adsorption within membrane matrix. This leads to a depletion of solute concentration in the concentration boundary layer and its thickness is reduced significantly.

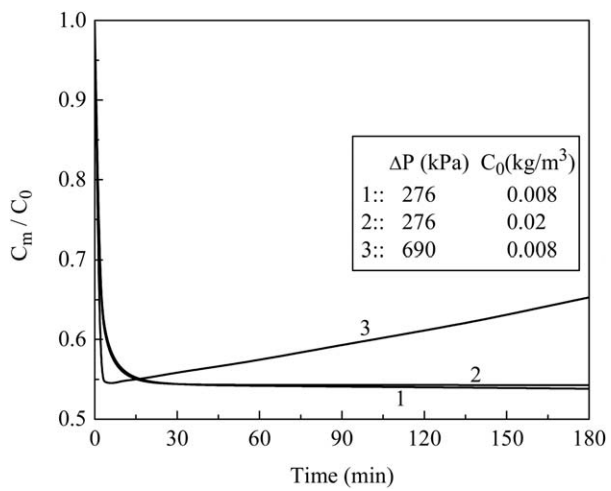

Figure 4. Variation of the membrane surface concentration for different operating conditions.

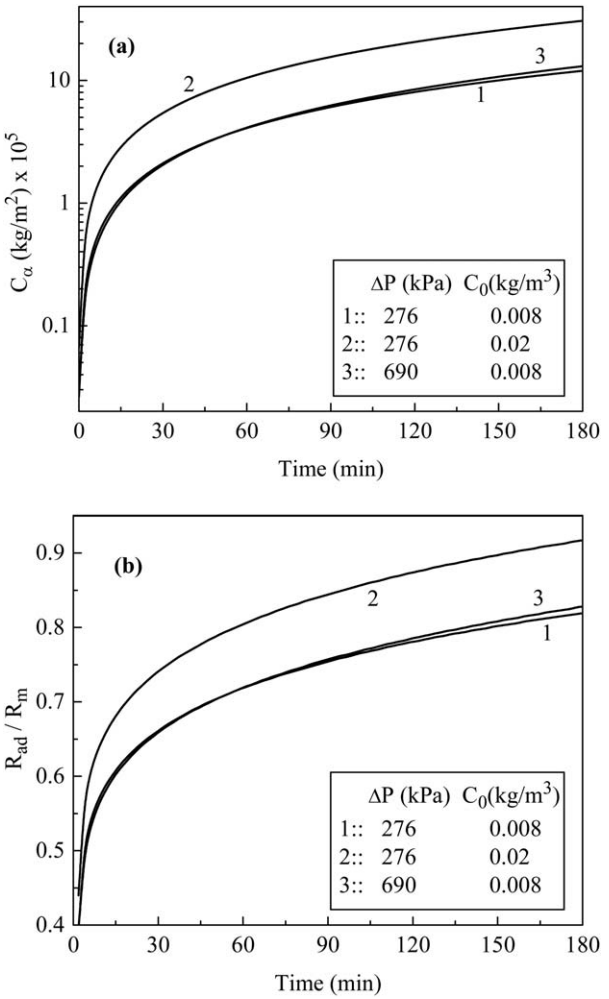

Figure 5. (a) Solute adsorption profile on the membrane surface and (b) adsorption resistance associated with the adsorption phenomena.

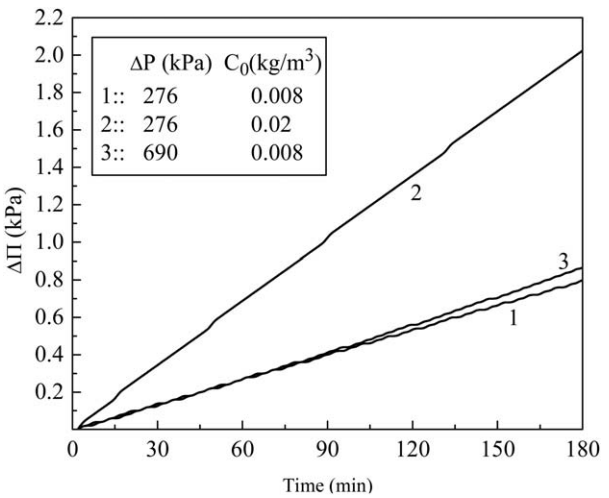

Figure 6. Osmotic pressure due to difference in solute concentration across the membrane.

Effects of TMP and feed concentration on the membrane surface concentration are presented in Figure 4. Effects of feed concentration are observed in curves 1 and 2. As discussed in the preceding paragraph, increase in feed concentration leads to accumulation of solute particles on the membrane surface and consequently, surface concentration increases. However, curves 1 and 2 almost superpose. This indicates that increase in feed concentration from 0.008 to 0.02 kg/m^3 (2.5 times increase) results to proportional increase in membrane surface concentration and hence, the profiles of nondimensional surface concentration coincide each other. The effect of TMP is observed by comparing the curves 1 and 3. At 276 kPa, membrane surface concentration decreases sharply up to 15 min due to strong adsorption and it remains almost invariant thereafter. This shows that beyond 15 min, adsorption occurred in the same rate. In case of higher TMP, more solutes are convected toward the membrane initially, thereby increasing the concentration gradient for adsorption. Thus, within few minutes of the starting of the filtration, membrane surface concentration decreases sharply indicating remarkably strong adsorption. After few minutes (about 2 min from curve 3), the rate of adsorption becomes slower and membrane surface concentration starts increasing. However, it increases from 0.55 to 0.65 after 3 h of filtration indicating within that period, adsorption is still dominant compared to concentration polarization. It can be noted from Figure 3 that for all the conditions, c_m/c_0 is always less than 1.0, showing the dominance of solute adsorption.

"c_α" indicates adsorbed solute per unit membrane surface area. The influence of the operating conditions on c_α are shown in Figure 5a. Curves 1 and 2 show the effect of feed concentration. As the feed concentration increases, more solutes are available for surface adsorption, thereby increasing its value. Conversely, it is observed from curves 1 and 3 that effect of TMP on c_α is marginal. With increase in TMP, concentration of solute at the membrane surface (c_m) increases as observed from Figure 3 (from 0.55 to 0.65 at 180 min). However, according to the dynamics of adsorption given by Eq. 14, this amount of increase in c_m results into marginal increase in concentration of adsorbed solute on the membrane surface. Thus, increase in TMP has less significant effect on solute adsorption in MMM compared to increase in feed concentration.

Figure 5b shows the effects of operating conditions or adsorption resistance. Because adsorption resistance is directly proportional to "c_α" (Eq. 18), the trends are similar to those in Figure 5a. However, it may be noted from Figure 5b, that after 3 h of filtration, adsorption resistance becomes almost comparable to membrane hydraulic resistance. This is a significant observation indicating the resistance due to concentration polarization is negligible in the case study of MMM. This point is proved more strongly from the observation presented in Figure 6.

The impact of osmotic pressure difference across the membrane is shown in Figure 6. The general observation from the curves in this figure shows that the osmotic pressure difference across the membrane increases within filtration time but its value is negligible compared to those of TMP. Thus, the contribution of osmotic pressure on the overall flux decline mechanism (as represented in Eq. 7) is negligibly small compared to adsorption resistance and hydraulic resistance of the membrane. However, the effects

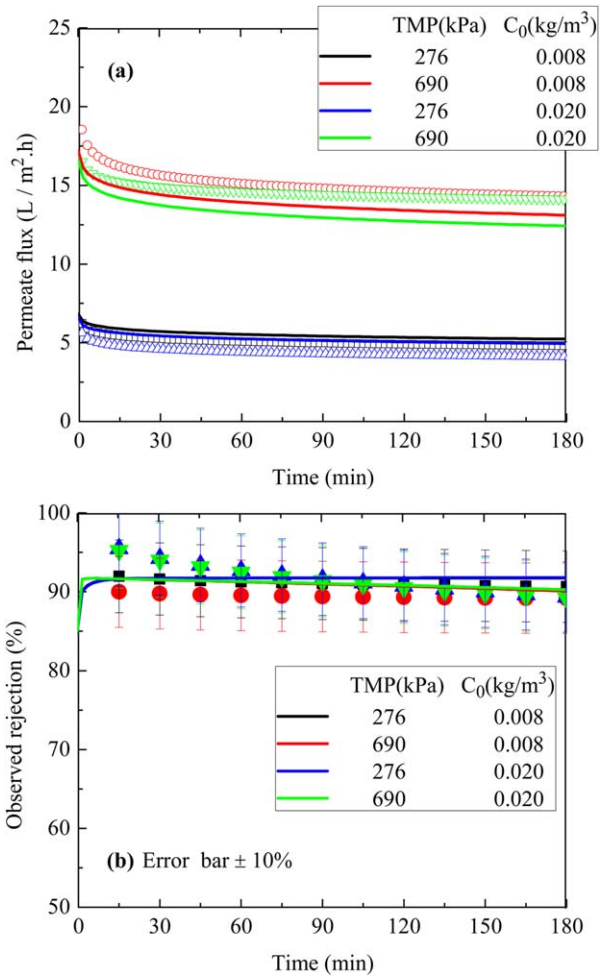

Figure 7. Experimental and simulated profiles of (a) permeate flux and (b) retention of fluoride contaminated solution at pH 7.0.

The symbols represent the experimental data points while the solid lines are for simulated results. [Color figure can be viewed in the online issue, which is available at wileyonlinelibrary.com.]

of feed concentration on osmotic pressure difference are much stronger than TMP. These results are in direct corroboration of the profiles of membrane surface concentration shown in Figure 4.

Comparison between the experimental flux and rejection profiles for fluoride removal in CAP-activated alumina MMM is presented in Figure 7. It can be observed from both the figures that the calculated values are within ±10% of the experimental results. Similarly, the comparison between the experimental and the calculated profiles of permeate flux and observed rejections are shown in Figure 8 for filtration of catechol using CAP-alumina nanoparticle-doped MMM. It can be observed from Figure 8a that the calculated flux profile matches pretty well with the experimental data. The calculated fluxes are within ±10% of the experimental results for the entire duration of filtration. It is to be noted from Figure 8b that at lower TMP, the profiles of observed rejection match within ±10% of the experimental results. But, for higher TMP, 690 kPa, the observed retention deviates more than 10% beyond 90 min of filtration period. In case of CAP-alumina nanoparticle MMM, the membrane

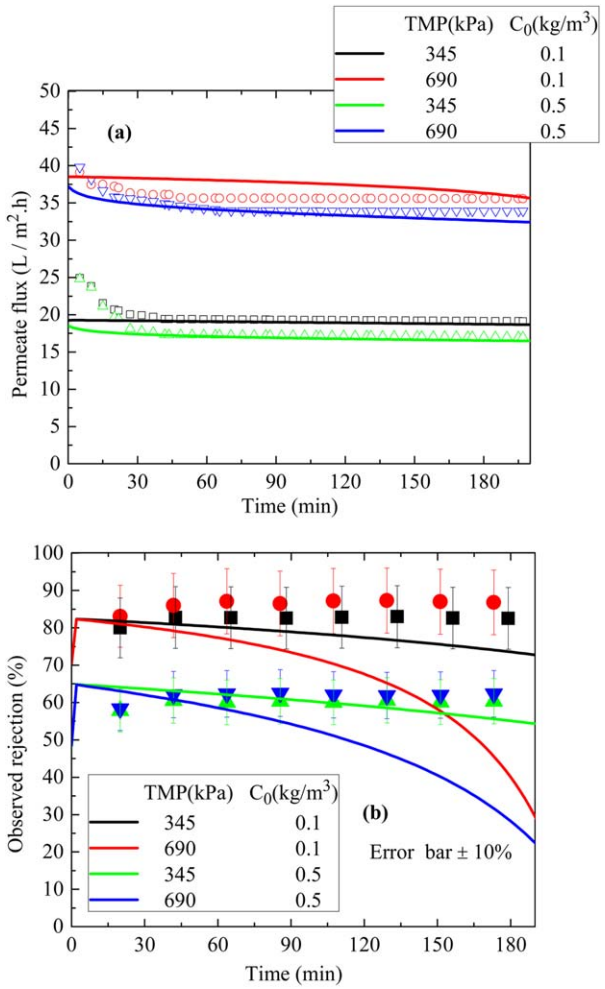

Figure 8. Experimental and simulated profiles of (a) permeate flux and (b) retention of catechol solution at pH 8.3.

The symbols represent the experimental data points while the solid lines are for simulated results. [Color figure can be viewed in the online issue, which is available at wileyonlinelibrary.com.]

surface becomes significantly charged.[23] Thus, there exists charge–charge interaction between solutes and the membrane surface. It is believed that such effect becomes prominent at higher TMP. Because such phenomena are not included in this model, the model predictions could not capture the experimental trend beyond certain time of filtration, when these charge interactions becomes significant.

The magnitude of the isotherm constants severely affects the system performance, that is the permeate flux and observed retention, as expressed in Figure 9. The variation of permeate flux with the isotherm constants are shown in Figure 9a. The effects of adsorption capacity "*A*" on the permeate flux are summarized in curves 1 and 3. As the value of "*A*" increases 100-folds, it leads to quite strong adsorption of solute by the membrane, thereby increasing adsorption resistance and hence, permeate flux is lowered in curve 3 compared to curve 1. Increasing the constant "*B*," leads to lowering in solute adsorption thereby, decreasing adsorption resistance and enhancing permeate flux compared to curve 1. Trends of observed retention are shown in Figure 9b. Increase in "*A*" indicates strong solute adsorption (compare curves 1 and 3). Therefore, solute retention is very high and as shown in curve 3, it is close to 100% from 30 min onward. Conversely, when "*B*" is increased, adsorption is less and more solutes permeate through the membrane, thereby decreasing the observed retention. Thus, observed retention decreases from 82 to 77% as the "*B*" increases 100-folds (comparing curves 1 and 2).

Effects of the parameters responsible for adsorption kinetics on system performance are shown in Figure 10. Variations of permeate flux and observed rejection are shown in Figures 10a, b, respectively. Effects of parameter k and n (in Eq. 18) are shown by curves 1 and 2, and 1 and 3. As evident from Eq. 18, increase in k indicates increase in adsorption resistance. Thus, increase in k from 10^{14} to 10^{15} results into a corresponding decrease in permeate flux from 10 to 2.5 L/m^2 h. Similarly, n being a fraction, increase in n results in decrease of adsorption resistance, R_{ad} and consequently increase in permeate flux. For example, the permeate flux increases from 12 to 22 L/m^2 h as the value of n increases from 0.1 to 0.5. Effects of α_1 and α_2 (in Eq. 14) on permeate flux are observed by comparing curves 1 and 4, and 1 and 5. Rate of change in concentration of adsorbed solute on membrane surface is presented by the parameter α_1. A closer look into Eq. 14 reveals that increase in α_1, results to increase in c_α, and hence adsorption resistance and subsequently, decrease in permeate flux. This is evident by

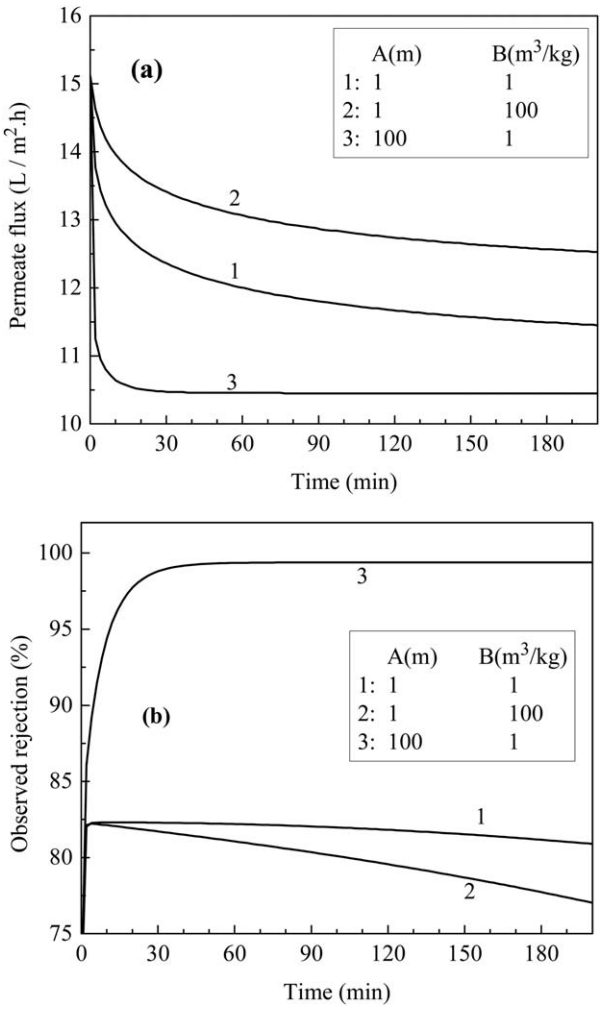

Figure 9. Simulated profiles of the (a) permeate flux and (b) rejection for different values of the adsorption isotherm constants.

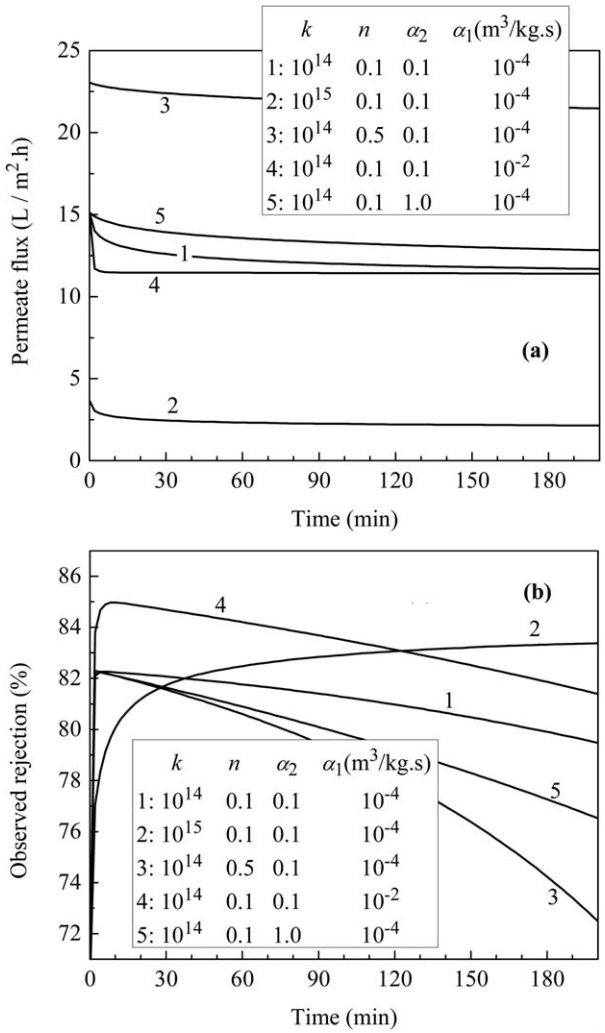

Figure 10. Simulated profiles of the (a) permeate flux and (b) rejection for different values of the model parameters.

comparing curves 1 and 4. Because α_1 dictates the rate of change of c_α (Eq. 14), increase in α_1 from 10^{-4} and 10^{-2} leads to rapid decrease in permeate flux (curve 4). However, after 1 h of filtration time, effects of α_1 becomes marginal and both the flux profiles almost coincide. Effect of α_2 on permeate flux is complex and it depends on the variation of membrane surface concentration (c_m) and adsorbed solute concentration on membrane surface (c_α). Increase in α_2 results to enhanced c_m, leading to lower amount of c_α. This leads to lower adsorption resistance and high-permeate flux. However, within the range of parameter α_2, this increment in not significant. As α_2 increases from 0.1 to 1.0, permeate flux increases from 12 to 14 L/m^2 h.

The corresponding effects on observed rejection are shown in Figure 10a. Increase in k results to more solute adsorption and hence, observed rejection increases. At the end of 3 h filtration, R_0 increases from 80 to 84% as k increases from 10^{14} to 10^{15}. As already discussed, increase in n leads to reduction in solute adsorption. Thus, observed rejection decreases from 80 to 74%, as n increases from 0.1 to 0.5. Effects of α_1, are evident from curves 1 and 4. As α_1 increases from 10^{-4} to 10^{-2}, it leads to more adsorption and thus improving R_0 from 80 to 83% after 3 h of filtration. Similarly, increase in α_2 from 0.1 to 1.0 leads to lowering in adsorption and hence, the observed retention. The value of R_0 decreases from 80 to 78% after 3 h, comparing curves 1 and 5.

Conclusions

Adsorption of solutes in membrane matrix during ultrafiltration of MMM plays an important role. In such cases, adsorption on membrane matrix becomes stronger compared to convection-diffusion led concentration polarization. This can be confirmed by the value of membrane surface concentration which is always less than feed concentration. However, concentration polarization increases with feed concentration and TMP drop, as expected. The magnitude of concentration boundary layer (δ) decreases by 2.5 times with increase in TMP from 276 to 690 kPa, in the case fluoride ultrafiltration. Increase in feed concentration has a stronger effect on solute adsorption on the membrane surface and adsorption resistance, compared to increase in TMP drop. Effects of osmotic pressure in case of filtration of smaller sized solutes on MMM are negligible compared to TMP drop. The developed model adequately captures the rejection dynamics of the solute and variation of feed volume and bulk concentration with time. The model predicts experimental data of permeate flux and observed rejection with adequate accuracy and matches within $\pm 10\%$ of the experimental results. Parametric variation of various adsorption constants is also simulated and their effects on system performance have been quantified. The rejection increases by 25% on increasing the Langmuir constant (A) by 100-folds while permeate flux decreases by 10%.

Acknowledgments

This work is partially supported by a grant from the Board of Research in Nuclear Sciences (BRNS), Department of Atomic Energy, Government of India, Mumbai, under the scheme no. 2012/21/03-BRNS, dated 25-07-2012 and by Department of Science and Technology, New Delhi, Government of India, under the scheme DST/TMC/2K11/339, dated 23-05-2012. Any opinions, findings and conclusions expressed in this paper are those of the authors and do not necessarily reflect the views of BRNS or DST.

Notation

A = Langmuir isotherm constant in Eq. 15, m
a_0, = a_1, a_2 = coefficients in Eq. 27
A_m = available membrane surface area for filtration, m^2
B = Langmuir isotherm constant in Eq. 15, m^3/kg
c = concentration, kg/m^3
c^* = nondimensional concentration, c/c_0
c_0 = initial feed concentration, kg/m^3
c_α = amount of solute adsorbed on membrane surface, kg/m^2
c^*_α = nondimensional amount of solute adsorbed, $c_\alpha/R\ c_0$
c_b = bulk feed concentration, kg/m^3
c^*_b = nondimensional bulk concentration, c_b/c_0
c_e = equilibrium concentration at the membrane surface, kg/m^2
c_m = solute concentration at membrane surface, kg/m^3
c^*_m = nondimensional membrane surface concentration, c_m/c_0
c_p = permeate concentration of solute, kg/m^3
c_{pm} = interface permeate concentration as described in Figure 1, kg/m^3
D = diffusivity of solute, m^2/s
k = modified adsorption resistance model constant, defined in Eq. A4
k' = adsorption resistance model constant in Eq. 18, m^{3n-1} kg^{-n}
k_a = Langmuir isotherm constant specified in Eq. 16, m^3/kg
L = thickness of the membrane, m

L_p = permeability of the membrane, m/Pa s
M_w = molecular weight of the solute, g/mol
n = power coefficient adsorption resistance model in Eqs. 18 and A4
N_d = number of data points in the ith experiment
N_{exp} = total number of experiments using a particular membrane-solute system
Pe_w = nondimensional permeate flux, $v_w R/D$
q_e = amount of solute adsorbed at equilibrium by the adsorbent, kg/kg
R = radius of the experimental batch cell, m
$R_{0,exp}$ = experimental observed rejection
R_{ad} = resistance to solvent flux due to adsorption, m^{-1}
R^*_{ad} = nondimensional adsorption resistance, R_{ad}/R_m
R_g = universal gas constant, J/mol K
R_m = membrane hydraulic resistance, m^{-1}
R_r = real retention of the membrane
R_{r1} = interface real retention of the membrane, described in Figure 1
R_{r2} = interface real retention of the membrane, described in Figure 1
S_1 = objective function for minimizing the sum of the relative error between experimental and theoretical permeate flux
S_2 = objective function for minimizing the sum of the relative error between experimental and theoretical observed rejection values
T = temperature of the system, K
t = time of filtration, s
v = axial velocity component in Eq. 1, m/s
V = volume of feed, m^3
V^* = nondimensional bulk volume, V/V_0
V_0 = initial feed volume, m^3
V_m = Langmuir isotherm constant specified in Eq. 16, kg/kg
v_w = permeate velocity, m/s
$v_{w,exp}$ = experimental permeate flux data, L/m^2 h
y = local cartesian y coordinate, m
y^* = nondimensional axial coordinate, y/R

Greek letters

α_1 = model constant in Eq. 14, m^3/kg s
α_2 = model constants in Eq. 14
δ = thickness of the mass-transfer boundary layer, m
δ^* = nondimensional mass-transfer boundary layer
ΔP = transmembrane pressure drop, Pa
$\Delta\pi$ = osmotic pressure difference across the membrane, Pa
ε = porosity of the membrane
γ^+, γ^- = Vant-Hoff's factor for positive and negative ions species in solution
μ = viscosity of the solution, Pa s
π = osmotic pressure of the solution, Pa
ρ_{memb} = density of the membranes, kg m^3
τ = nondimensional time of filtration, $t\,D/R^2$

Literature Cited

1. Ismail AF, Matsuura T, editors. *Sustainable Membrane Technology for Energy, Water and Environment*. New Jersey: Wiley, 2012.
2. Majeed S, Fierro D, Buhr K, Wind J, Du B, Boschetti-de-Fierro A, Abetz V. Multi-walled carbon nanotubes (MWCNTs) mixed polyacrylonitrile (PAN) ultrafiltration membranes. *J Membr Sci*. 2012; 403–404:101–109.
3. Chung TS, Jiang LY, Lia Y, Kulprathipanja S. Mixed matrix membranes (MMMs) comprising organic polymers with dispersed inorganic fillers for gas separation. *Prog Polym Sci*. 2007;32:483–507.
4. Hoek EMV, Ghosh AK, Huang X, Liong M, Zink JI. Physical–chemical properties, separation performance, and fouling resistance of mixed-matrix ultrafiltration membranes. *Desalination*. 2011;283: 89–99.
5. Tijink MSL, Wester M, Sun J, Saris A, Bolhius-Versteeg LAM, Saiful S, Joles JA, Borneman Z, Wessling M, Stamatialis DF. A novel approach for blood purification: Mixed-matrix membranes combining diffusion and adsorption in one step. *Acta Biomater*. 2012;8:2279–2287.
6. De S, Bhattacharjee S, Sharma A, Bhattacharya PK. Generalized integral and similarity solutions of the concentration profiles for osmotic pressure controlled ultrafiltration. *J Membr Sci*. 1997;130: 99–121.
7. Mondal S, Rai C, De S. Identification of fouling mechanism during ultrafiltration of stevia extract. *Food Bioprocess Technol*. 2013;6: 931–940.
8. De S, Bhattacharjee S. Flux decline during cross flow membrane filtration of electrolytic solution in presence of charged nano-colloids: a simple electrokinetic model. *J Colloid Interface Sci*. 2011;353: 530–536.
9. Mondal S, De S. Generalized criteria for identification of fouling mechanism under steady state membrane filtration. *J Membr Sci*. 2009;344:6–13.
10. Matthiasson E. The role of macromolecular adsorption in fouling of ultrafiltration membranes. *J Membr Sci*. 1983;16:23–36.
11. Doshi MR. Limiting flux in the ultrafiltration of macromolecular solutions. In: Sourirajan S, Matsuura T, editors. *Reverse Osmosis and Ultrafiltration*, Vol. 281. Washington, DC: ACS Symposium series, 1985:209–223.
12. Gekas V, Aimar P, Lafaille JP, Sanchez V. A simulation study of the adsorption-concentration polarization interplay in protein ultrafiltration. *Chem Eng Sci*. 1993;48:2753–2765.
13. Ruiz-Bevia F, Gomis-Yagues V, Fernandez-Sempere J, Fernfindez-Torres MJ. An improved model with time-dependent adsorption for simulating protein ultrafiltration. *Chem Eng Sci*. 1997;52:2343–2352.
14. De S, Bhattacharjee S, Sharma A, Bhattacharya PK. Generalized integral and similarity solutions of the concentration profiles for osmotic pressure controlled ultrafiltration. *J Membr Sci*. 1997;130: 99–121.
15. Cheryan M. *Ultrafiltration and Microfiltration Handbook*. Lancaster: Technomic Publishing, 1998.
16. Mondal S, Mlouka SB, Dhahbi M, De S. A physico-chemical model for polyelectrolyte enhanced ultrafiltration. *J Membr Sci*. 2011;376: 142–152.
17. Vilker VL, Colton CK, Smith KA. The osmotic pressure of concentrated protein solutions: effect of concentration and pH in saline solutions of bovine serum albumin. *J Colloid Interface Sci*. 1981;79: 548–566.
18. Mondal S, Cassano A, Tasselli F, De S. A generalized model for clarification of fruit juice during ultrafiltration under total recycle and batch mode. *J Membr Sci*. 2012;366:295–303.
19. Shampine LF, Reichelt MW, Kierzenka JA. Solving Index-1 DAEs in MATLAB and Simulink. *SIAM Rev*. 1999;41:538–552.
20. Mondal S, Chhaya, De S. Prediction of ultrafiltration performance during clarification of stevia extract. *J Membr Sci*. 2012;396:138–148.
21. Mondal S, Chhaya, De S, Modeling of cross flow ultrafiltration of stevia extract in a rectangular cell. *J Food Eng*. 2012;112:326–337.
22. Byrd RH, Gilbert JC, Nocedal J. A trust region method based on interior point techniques for nonlinear programming. *Math Program*. 2000;89:149–185.
23. Mukherjee R, De S. Adsorptive removal of phenolic compounds using cellulose acetate phthalate-alumina nanoparticle mixed matrix membrane. *J Hazard Mater*. 2014;265:8–19.
24. Ramos RL, Utrilla JR, Castillo NAM, Polo MS. Kinetic modeling of fluoride adsorption from aqueous solution onto bone char. *Chem Eng J*. 2010;159:458–467.
25. Choi SK, Scura F, Barbieri G, Mazzei R, Giorno L, Drioli E, Kim JH. Bio-degradation of phenol in wastewater by enzyme-loaded membrane reactor: numerical approach. *Membr J*. 2009;19:72–82.
26. Chatterjee S, De S. Adsorptive removal of fluoride by activated alumina doped cellulose acetate phthalate (CAP) mixed matrix membrane. *Sep Purif Technol*. In press.
27. Field RW, Aimar P. Ideal limiting fluxes in ultrafiltration: comparison of various theoretical relationships. *J Membr Sci*. 1993;80:107–115.

Appendix A

The flux equation at the interface (Eq. 5) in nondimensional form is obtained by substituting the expression of $\frac{dc*}{dy^*}|_{y*=0}$ from Eq. 28 and from the definition of real retention (Eq. 21)

$$Pe_w c^*_m R_r = -2\left(\frac{c^*_m - c^*_b}{\delta *}\right) + \frac{dc^*_\alpha}{d\tau}|_{y*=0} \tag{A1}$$

where $c^*_\alpha = \frac{c_\alpha}{c_0 R}$. To compute $\frac{dc^*_\alpha}{d\tau}|_{y*=0}$, Eq. 14 is evaluated at $c^* = c^*_m$, which is expressed in nondimensional form as

$$\frac{dc^*_{\alpha}}{d\tau}|_{y*=0} = \frac{\alpha_1 R^2}{D} c_0^{\alpha_2} c_m^{*\,\alpha_2} \left[c^*_e|_{y*=0} - c^*_m \right] \quad \text{(A2)}$$

Similarly, equilibrium concentration at the interface $\left(c^*_e|_{y*=0}\right)$ in nondimensional form in expressed as

$$c^*_e(\tau)|_{y*=0} = \frac{A c^*_m}{R\left(1+Bc_0 c^*_m\right)} \quad \text{(A3)}$$

The adsorption resistance is also transformed into nondimensional form as

$$R^*_{ad} = \frac{R_{ad}}{R_m} = k\ \left(c^*_{\alpha}\right)^n \quad \text{(A4)}$$

where $k\ = \frac{k/}{R_m}\left(c_0 R\right)^n$

The expression for nondimensional permeate flux (Pe_w) can be obtained from Eq. 6 as

$$Pe_w = L_p \Delta P \frac{R}{D}\left(1 - \frac{\Delta\pi}{\Delta P}\right) \frac{1}{\left[1+R^*_{ad}\right]} \quad \text{(A5)}$$

where L_p represents the membrane permeability $\left(L_p = \frac{\Delta P}{\mu R_m}\right)$. The nondimensional form of Eq. 11 and 12 are represented as

$$V^* \frac{dc^*_b}{d\tau} + c^*_b \frac{dV^*}{d\tau} + \left(\frac{RA_m}{V_0}\right) \frac{dc^*_{\alpha}}{d\tau} + c^*_m (1-R_r)\left(\frac{RA_m}{V_0}\right) = 0 \quad \text{(A6)}$$

$$\frac{dV^*}{d\tau} = -Pe_w \left(\frac{A_m R}{V_0}\right) \quad \text{(A7)}$$

Manuscript received Nov. 8, 2013, and revision received Jan. 13, 2014.